Measurement 136 (2019) 647–657

Contents lists available at ScienceDirect

Measurement

journal homepage: www.elsevier.com/locate/measurement

Development and characterization of air kerma cavity standard

M.M. Szymko *, L. Michalik, A.B. Knyziak, A.W. Wójtowicz

Central Office of Measures, Elektoralna 2 Str., 00-139 Warsaw, Poland

ARTICLE INFO

Article history:
Received 15 October 2018
Received in revised form 10 December 2018
Accepted 7 January 2019
Available online 8 January 2019

Keywords:
Air kerma cavity standard
Ionization chamber
Gamma radiation
Monte Carlo simulation

ABSTRACT

Ionization chambers are the most common detectors for precise measurements such as these required in radiation protection and radiotherapy. This paper presents the design, development and characterization of a new graphite-walled cavity ionization chamber used as a primary standard for air kerma rate for ^{137}Cs and ^{60}Co gamma radiation of the Central Office of Measures (GUM). The paper describes particularly methods for a cavity volume determination and the cavity volume relation to an electric field. The various correction factors to be applied to the primary standards and their determination by experimental and Monte Carlo methods are discussed. Re-evaluation of the standard according to the recommendations of ICRU90 Report for the new primary standard is presented. A typical uncertainty budget for the graphite-walled cavity ionization chamber as a primary standard for air kerma rate for gamma radiation is presented and results of internal comparisons between standards are summarized and discussed.

1. Introduction

In the field of ionizing radiation the air kerma is one of the basic quantities commonly used in dosimetry. Primary standards for air kerma rate for ^{137}Cs and ^{60}Co gamma radiation are based on a graphite-walled cavity ionization chambers. For gamma radiation these ionization chambers generally present spherical, cylindrical or plane-parallel design. The use of the heat-shrink tubing as the insulator simplified the chamber design and assembling. This original solution gives good electrical properties, dimensional stability and high resistance to radiation relevant for primary standard.

Ionization chambers present some advantages such as: small size, easy to use and they could measure multi-directional irradiation fields. In the characterization process of the cavity ionization chambers some experiments and Monte Carlo simulations need to be undertaken. The Monte Carlo method has proven to be invaluable for radiation transport simulations, specially to determine the correction factors of the ionization chambers characterized as primary standards. Besides that, it is widely considered that a reliable computational measure can substitute a physical experiment where direct measurements are not possible.

This paper presents the design, development and characterization of a new graphite–walled cavity ionization chamber that potentially will be used as a new primary standard for air kerma rate for ^{137}Cs and ^{60}Co gamma radiation of the Central Office of Measures (GUM). It describes a design of the graphite-walled cavity ionization chamber, methods of cavity volume determination and cavity volume relation to electric field in Sections 2 and 3. The various correction factors to be applied to the primary standards and their determination by experimental and Monte Carlo methods are discussed in Sections 4 and 5. A typical uncertainty budget for a graphite-walled cavity ionization chamber as primary standard for air kerma rate for gamma radiation is presented. Results of internal comparisons between standards and the re–evaluation of the standard according to the recommendations of ICRU90 Report for the new primary standard are presented in Section 6.

2. New primary kerma standard

The new primary standard for air kerma rate for ^{137}Cs and ^{60}Co gamma radiation of the Central Office of Measures (GUM) is a graphite-walled cavity ionization chamber designed and constructed by one of the authors, referenced as IGNAS-IC16A#001 (Fig. 1). The chamber body was assembled from three graphite components: bottom, central electrode and cylindrical cap. A crucial element was the determination of the cavity volume. A high-accuracy coordinate measuring machine at the GUM was used to measure these three components before assembly, as is described in Section 2.3. The polarizing potential of +300 V was applied in the wall.

2.1. Construction of the cavity chamber

All elements of the prototype chamber have been close-fitted or threated together without using any glue. Main components are

* Corresponding author.
E-mail address: magdalena.szymko@gum.gov.pl (M.M. Szymko).

https://doi.org/10.1016/j.measurement.2019.01.010
0263-2241/

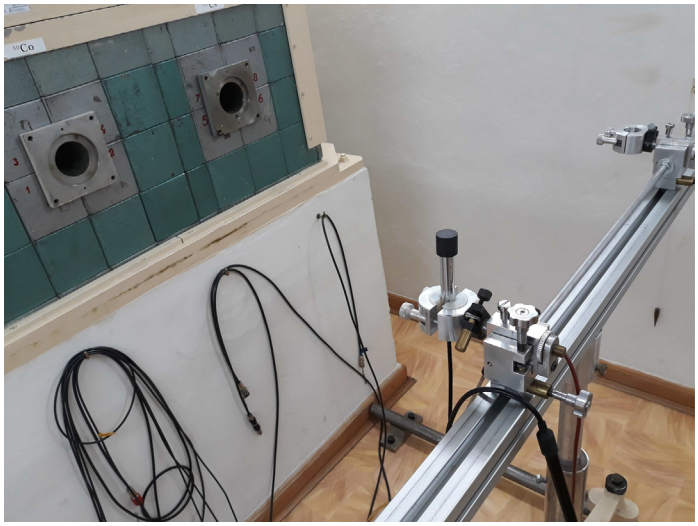

Fig. 1. The prototype ionization chamber type IGNAS-IC16A#001 in the test facility.

wall and central electrode made of ultra-pure graphite, guard electrode made of ultra-pure aluminum, insulating material, venting holes on the both sides between the chamber wall and the stem, electrical connections to the wall and the central electrode and stem. All elements are shown in Fig. 2. The graphite that was used has a density of 1.81 g/cm^3 and the 99.997% purity. The chamber wall has a thickness of 4 mm and the electrode has a diameter of 2 mm and 10 mm height. The nominal wall thickness of 4 mm is sufficient to establish transient CPE for ^{137}Cs and ^{60}Co gamma radiation. The chamber has nominal inner height of 11 mm and diameter of 11 mm. An insulator material of the prototype chamber is heat-shrink tubing of 4 kV with wall of 0.25 mm thickness made of polyethylene of 0.94 g/cm^3 density. Extra care was taken to ensure that the insulator surfaces were clean and smooth. To separate the guard ring from the insulator and reduce the surface effects an air gap of 0.25 mm thickness with a length of 6 mm was made from a top of the guard electrode. Air pressure equilibrium between the inside and the outside of the cavity is reached through two symmetrical holes in the graphite part of the stem. The cavity is surrounded almost completely by graphite with only a small amount of insulating material visible at the bottom of the central electrode. This is a relevant issue since materials different from graphite disturb the conditions required for a Bragg-Gray cavity.

2.2. Electric field inside the chamber

In cylindrical cavity chambers, where two conducting surfaces meet at an angle of 90°, the effective collecting volume is smaller than a geometric volume of the cavity because an electric field strength in close proximity to the corners of the graphite cap is approximately null. Charged particles generated in those regions will therefore not contribute to the collected ionization current. Electric-field calculations using the finite-element method obtained by FreeFEM++ showed that there are small 'dead regions', in other words, that not all produced ions can be transported to the electrodes, as shown in Fig. 3. To unify the collecting and the geometrical volume chamber shape should be spherical, thought spherical shape causes difficulties in the volume evaluation hence determines higher uncertainty (as is discussed in [1]). The guard electrode effect was also investigated in FreeFEM++ calculations, but it was found negligible.

2.3. Cavity volume determination

The individual components of the cavity chamber assembly were measured in the Precise Geometric Measurements Section of the Length Laboratory at Central Office of Measures (GUM) using the coordinate measuring machine (SIP type CMM5, serial number

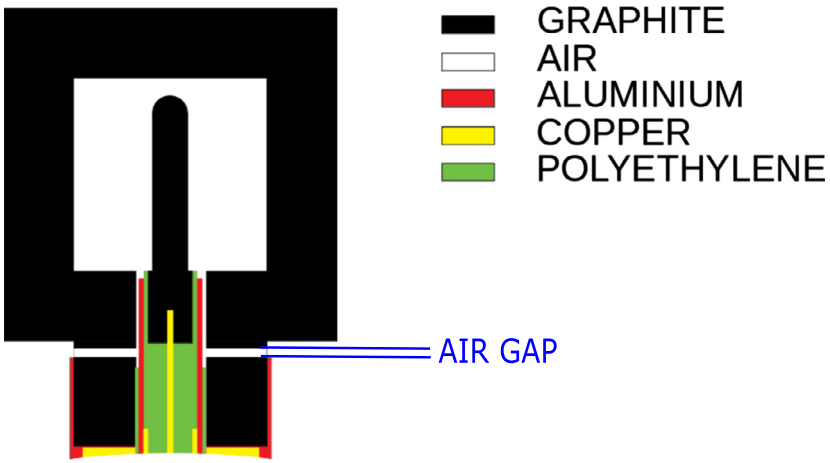

Fig. 2. Scheme of the prototype ionization chamber type IGNAS-IC16A#001 cross-section with marked materials used for construction. (For interpretation of the references to colour in this figure legend, the reader is referred to the web version of this article.)

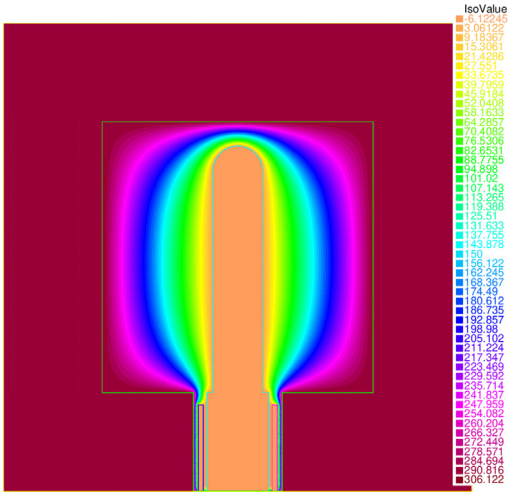

Fig. 3. Electric field inside a cylindrical chamber calculated using the finite element analysis. (For interpretation of the references to colour in this figure legend, the reader is referred to the web version of this article.)

302). Most of length parameters were measured on a CMM fitted with a contacting probe system, only the diameter of central electrode was measured with the OLYMPUS vision system. The probe system was fitted with a two-millimeter diameter stylus and contacted the surfaces to be measured with a force of 0.05 N. The size of the stylus was the smallest currently available, yet allowing to test finest detail of the geometric structure. The cavity chamber dimensions as shown in the Fig. 4 are summarized in Table 1. To determine the chamber collecting volume method of subsequent approximations was used. The simplest model (I) from Eq. (1) to get the chamber collecting volume was to subtract overall chamber volume V_{ch} and the volume of electrode V_{el} calculated from the measured dimensions.

$$\begin{aligned} &(I) \quad V = V_{ch} - V_{el} \\ &(II) \quad V = V_{ch} - V_{el} + V_{gap} \\ &(III) \quad V = V_{ch}^{A} + V_{ch}^{B} + V_{ch}^{C} - V_{el} + V_{gap} \end{aligned} \tag{1}$$

Table 1
The cavity chamber dimensions.

Measurand symbol	Measurand estimate in mm	Standard uncertainty in mm	Measurand relative error
D_A	10.991	0.001	0.009%
H_A	3.669	0.006	0.160%
D_B	10.976	0.001	0.009%
H_B	3.700	0.006	0.159%
D_C	10.986	0.001	0.009%
H_C	3.700	0.006	0.159%
h	9.497	0.010	0.103%
d_1	1.975	0.019	0.979%
d_2	2.007	0.034	1.698%
d_3	15.032	0.001	0.007%
h_1	2.008	0.006	0.290%
B	2.000	0.001	0.050%

Next approximation (II) includes also an additional volume V_{gap} of a gap between the plain cap and the threaded chamber base (Fig. 2). The gap width was measured three times and the mean gap width was calculated. The cap was then removed, pushed back onto the threaded base and the height measurements were repeated. The assembly height gives repeatability of closing on the level of 0.014 mm. The third (III) more detailed model was obtained taking into account that the cylindrical shape of the chamber is not ideal, and the chamber volume V_{ch} was divided in tree cylindrical slices which internal diameter was measured at tree different heights. This approach can be used in the future to improve uncertainty and the volume calculation, slicing the chamber finely. Another way to improve geometrical volume results could be a possibility to measure chamber parts on different stages of chamber assembling. The weight method of determining the chamber overall volume was also used (as in [1]). The empty chamber plain cap was weighted and then filled with distilled water of known density (in established temperature, pressure and humidity conditions) and weighted again. The water volume (ergo the chamber volume) was calculated from mass subtraction and known water density, the water absorption effect has been taken into account. To obtain collecting volume the electrode volume was subtracted and the gap volume was added (both values calculated from dimension measurement). Results for used methods with associated uncertainties were summarized in Table 2. The collecting volume obtained by

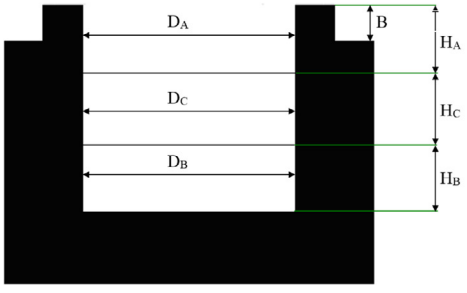

(a) The chamber volume V_{ch} divided in tree cylindrical slices: V_{ch}^{A}, V_{ch}^{B}, V_{ch}^{C} with diameters D^{A}, D^{B}, D^{C} and heights H^{A}, H^{B}, H^{C} respectively.

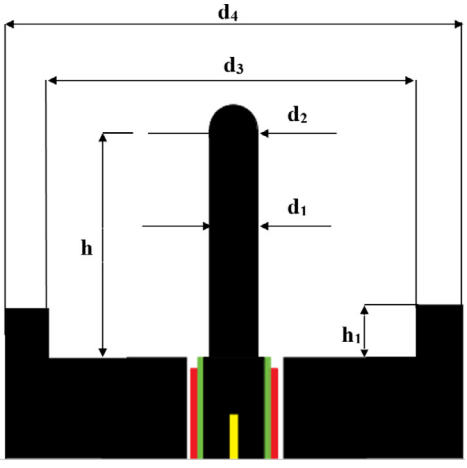

(b) The threaded chamber base dimensions symbols.

Fig. 4. The chamber geometry with measurand symbols. All measurand values are listed in Table 1.

Table 2
Results obtained from different methods of determining the chamber collecting volume.

Method	Volume/mm^3	Relative uncertainty
Geometrical (model III)	1019.058	0.15%
Weight	1013.497	0.20%

weight method differs from that obtained by other methods. A reason for that is a water surface tension causing a concave meniscus and disturbing water to fill exact volume of the chamber. This phenomenon has to be strongly considered if the weight method is used to determine volume of a spherical shape chamber. One of the known solution is to use mercury instead of water. In that case a meniscus is convex for the cylindrical-shape chamber and it is possible to remove it by cutting off form the surface. In the case of spherical shape cutting the meniscus is not possible in a neck region but it can be possible if measuring the volume of two hemispheres separately. However,then the volume uncertainty increases because of the hemispheres connection issue. In the future all methods of determining the collecting volume of a various shape chambers will be studied in details and presented in a paper.

Further calculations adopt the collecting volume value of 1019.058 mm^3 with 0.15% uncertainty, obtained in detailed (III) method.

3. Measurements

During all measurements the graphite-walled ionization chamber was connected to a digital electrometer Keithley model 6517A with power supply for polarity voltage. The electrometer worked in an external charge-mode, implemented by an electrometer negative-feedback with an external feedback capacitor. The basic charge measuring scheme is to transfer the electrical charge from the chamber to be measured to a capacitor of known value and then to measure the voltage across the known capacitor. In practice the current I is determined from the measurement of output voltage U_{out}. The method uses accurate digital voltmeters which can be set to a sample-and-hold readings of U_{out} at preset time intervals. In this case the measured current I is calculated as $I = -C \cdot \Delta U_{out}/\Delta t$. For measurements of the environmental conditions digital thermometer Elmetron model PT-401, digital barometer Vaisala model PTB-200 and digital hygrometer Elmetron model PWT-401 were used. All measurements are controlled by a dedicated application installed on a PC. Its task is also data acquisition and calculations.

Two sources were used for the measurements: ^{137}Cs source of an actual activity of 3.83 TBq (for the reference date of May 19, 2018) and a field size of 16 cm diameter for reference distance 1 m and ^{60}Co source of 1.12 TBq activity (for the reference date of June 1, 2018) and field of 15.5 cm diameter at the reference distance.

3.1. Saturation

The saturation characteristic has been obtained using ^{137}Cs source. The ion current has been measured with different voltages applied. Results are shown in Fig. 5. The chamber working voltage value was set up as a balance between being on a voltage plateau and mitigating a leakage current value. These conditions were met for value of +300 V.

3.2. Leakage current

Not the whole value of the total current measured in the ionization chamber is an effect of an irradiation of the chamber and it has to be taken to account. Effects like an irradiation of a chamber insulator or a quality of the chamber construction are affecting the chamber overall response. During all measurements the procedure was to measure leakage current after irradiation and subtract it from the measured ionization current value.

To investigate the chamber stability the leakage current just after connecting the chamber to the power supply was measured. After some time (approximate 1 h) it saturates to the value of about −0.0078(2) pA.

The leakage current value after irradiation is −0.007(1) pA, what in the worst case scenario gives 0.3% of measured ionization current.

Measurements of the leakage current with electrometer without connected chamber showed that the electrometer contribution to the leakage current is significant. Obtained value of −0.0065(1) pA leads to the 'clear' chamber leakage current of the order of 0.001 pA.

3.3. Stability

The chamber response was tested in relation to its stability by exposing the prototype to ^{137}Cs and ^{60}Co radiation under established geometric configuration. The long-term stability has been

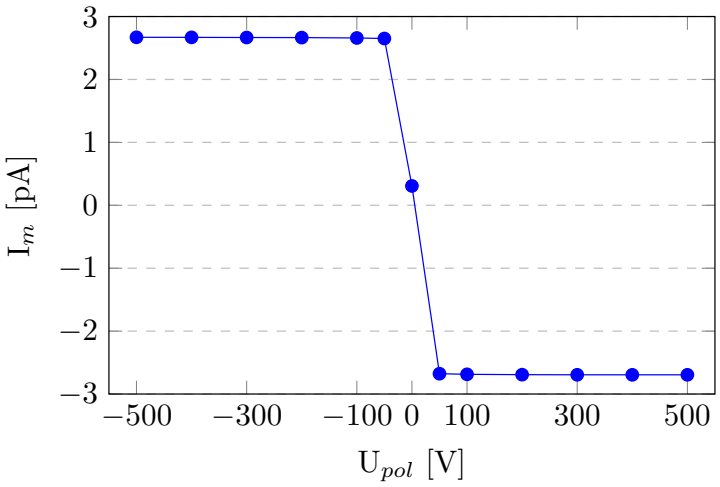

Fig. 5. Saturation curve of the prototype chamber for ^{137}Cs beam. The current uncertainty is less then 0.1%.

obtained by daily measurements of mean current corrected due to a leakage current, temperature and pressure conditions (more details in 4.1) and source decay. A correction factor for source decay k_t can be calculated as:

$$k_t = exp\left[\frac{ln2}{T_{1/2}}(t - t_0)\right] \tag{2}$$

with an uncertainty given by:

$$u_{k_t} = \frac{ln2}{T_{1/2}}\sqrt{u_t^2 + \left(\frac{t - t_0}{T_{1/2}}\right)^2 u_{T_{1/2}}^2} \tag{3}$$

where t is the measurements date, t_0 is the reference date (specified at the beginning of Section 3) and $T_{1/2}$ is the radioactive half-life for ^{137}Cs or ^{60}Co, respectively 30.05(8) years and 5.2711(8) years according to [2].

If any measurements were taken during one day the k_t factor wasn't taken into account. The uncertainty of the time of measurements u_t has been evaluated as 0.25 day.

Fig. 6 shows the study of the stability in the measured current. The normalized response is the ratio of ionization current measured daily and the mean value from all measurements taken during a few moths. Uncertainty is a standard combined uncertainty of a mean value uncertainty and uncertainty of corrected ionization current (including u_{k_t} from Eq. (3)).

During its lifetime the chamber has been reconstructed because of the volume measurement technique requirements (explained in 2.3). The long-term stability shows changes in the chamber response after reassembling. The reason for that divergence is a measurements routine. After reassembling the chamber a various tests were performed, involving changes in the applied voltage and other conditions, that could have an impact on the chamber response. Nevertheless measurements show that even in that case the chamber response variation is below 0.2% for both sources. For air kerma calculations in Section 6 only results of mid-term measurements (after reassembling) were taken into account.

3.4. Angular dependence

The angular dependence was obtained by measuring chamber response to radiation for five different rotation angles around the symmetry axis of the chamber. Normalized chamber response is the ionization current (with temperature and pressure correction) over a mean current value. Fig. 7 shows results for ^{137}Cs and ^{60}Co sources. In both cases deviation is below 0.2%.

3.5. Polarity correction

During routine measurements the ionization current was measured with positive working polarity. Polarity effect was investigated, therefore according to [3] it was expected to be negligible. From [3] the polarity correction factor is given by:

$$k_{pol} = \frac{|I_+| + |I_-|}{2I} \tag{4}$$

with an uncertainty that can be calculated as:

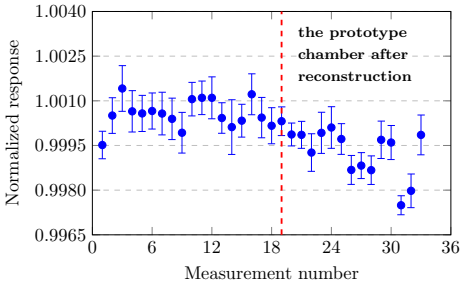

(a) ^{137}Cs, long-term measurements. After reconstruction stability was stored during various measurements with floating conditions therefore have noticeably different dispersion.

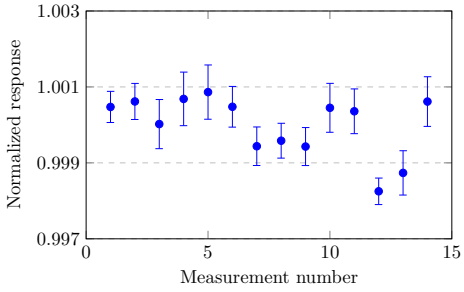

(b) ^{137}Cs, measurements after reassembling the chamber.

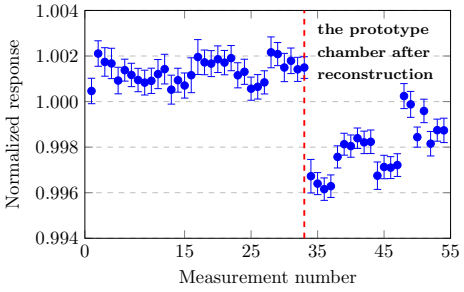

(c) ^{60}Co, long-term measurements. After reconstrution stability was stored during various measurements with floating conditions therefore have noticeably different dispersion.

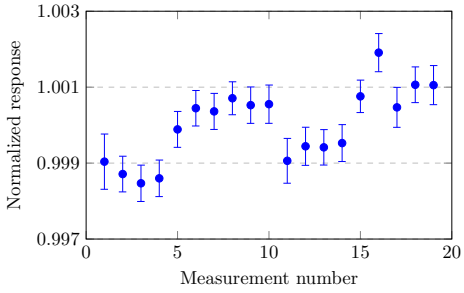

(d) ^{60}Co, measurements after reassembling the chamber.

Fig. 6. Normalized chamber response for ^{137}Cs and ^{60}Co source. Error bars represent expanded uncertainty with coverage factor of 2.

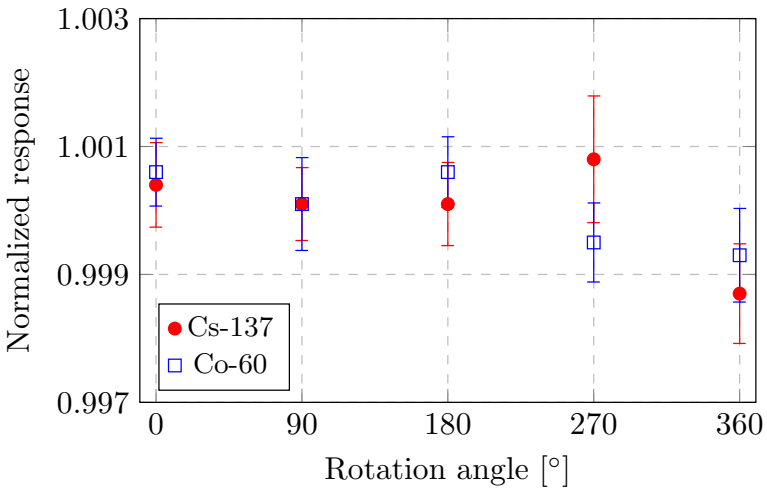

Fig. 7. Normalized chamber response due to rotation angle (around the symmetry axis of the chamber) for ^{137}Cs and ^{60}Co source. Error bars represent expanded uncertainty with coverage factor of 2.

$$u_{k_{pol}} = \frac{1}{2}\sqrt{\left(\frac{u_{I_-}}{I_+}\right)^2 + (2k_{pol}-1)^2\left(\frac{u_{I_+}}{I_+}\right)^2} \tag{5}$$

where I_+ and I_- are the ionization current measured with adequate polarity, and I is the ionization current with polarity used routinely.

According to Eq. (4) the ionization current was measured for opposite polarities in sequence: positive-negative-positive for both sources. The leakage current was measured after obtaining each single ionization current value. According to experimental results calculated value of correction factor for ^{137}Cs and ^{60}Co sources was respectively: $k_{pol}^{Cs} = 0.9999(4)$ and $k_{pol}^{Co} = 0.9999(3)$ for voltage +300 V. The polarity factor close to 1 proves high quality of the prototype chamber.

4. Air kerma rate measurements

The cavity theory for air kerma standards was summarized in [4] and can be expressed as the formula for measurable air kerma rates (with realistic cavity chambers and radiation fields) given by:

$$\dot{K}_{air} = \frac{I}{m_{air}}\left(\frac{\overline{W}}{e}\right)_{air}\left(\frac{\overline{\mu_{en}}}{\rho}\right)_{air,c}\bar{s}_{c,a}\frac{1}{1-\bar{g}_{air}}\cdot\prod_k \tag{6}$$

where I is the ionization current corrected to pressure and temperature conditions. The air mass $m_{air} = \rho_0 V_{col}$ is obtained for the air density ρ_0 at the reference conditions and for cavity volume V_{col} (determined as explained in Section 2.3). $\prod_k = k_h k_{rec} k_{stem} k_{wall} k_{an} k_{rn}$ corrects current for realistic conditions. The factors k_{pT}, k_h for pressure and temperature (air density) and humidity corrections are environmental-dependent values as described in Section 4.1. Factors for stem scatter correction k_{stem} and recombination losses correction k_{rec} were determined experimentally as described in Sections 4.3 and 4.4. Other factors like k_{wall}, k_{an} and k_{rn} for wall effects and beam non-uniformity corrections as well as the physical constants (values for stopping power $\bar{s}_{c,a}$, mass energy absorption coefficients $(\overline{\mu_{en}}/\rho)_{air,c}$ and bremsstrahlung losses $\bar{g}_{air}$) were calculated by Monte Carlo methods as described in Section 5.

4.1. Environmental correction factors

The air kerma rate value given by Eq. (6) depends on dry air mass (relative humidity $h_0 = 0\%$) in the reference conditions of temperature 20 °C and atmospheric pressure 1013.25 hPa. The cavity chamber is open to an ambient air, therefore a correction has to be made for realistic environmental conditions (p, T, h) influencing the air mass inside the ionization chamber. The temperature and pressure correction factor is introduced:

$$k_{pT} = \frac{273.15 + T}{293.15}\cdot\frac{1013.25}{p} \tag{7}$$

where $T/$°C is the measured temperature and $p/$hPa is the ambient pressure.

Humidity influence on the ionization chamber response and on correction factors was widely discussed in [5,6]. In conclusion, it is recommended (as in [3]) to use $k_h = 0.997$ for the relative humidity between 20% and 80% during measurements. This condition was preserved during measurements. Relative humidity various from 35% to 70%. Humidity was controlled during all tests and measurements. Fig. 8 shows some repeatable pattern in the ionization current and relative humidity values. For ^{137}Cs source (Fig. 6a) correlation is not so strong. It should be noted that the outline could be affected by measurement routine during the chamber testing (as was described in 3.3).

For ^{60}Co source also short-term stability in changing humidity conditions has been tested. Using simple dehumidifier it was possible to change humidity during measurements, from 53.2% to 41.3%. Relative humidity was measured continuously during this part of experiment. Fig. 9 shows the ionization chamber normalized response according to relative humidity. When humidity vary in the range of 10% normalized response variation is below 0.1%. Conclusion is that a relative humidity should be preserved on the same level during all measurements. Therefore, a system of controlling and stabilizing environmental conditions should be strongly recommended.

4.2. Attenuation correction

The attenuation corrector factor k_{att} compensates the beam attenuation due to air column between the source and the ionization chamber. It depends on the number of air molecules, hence depends on the ionization chamber distance from the source and the air pressure and temperature. The correction factor is given by:

$$k_{att} = exp\left[\left(\frac{\mu}{\rho}\right)_0(\rho_0 d_0)\left(\frac{1}{k_{pT}} - 1\right)\right] \tag{8}$$

where d_0 is the source-detector distance, ρ_0 is the air density in reference conditions.

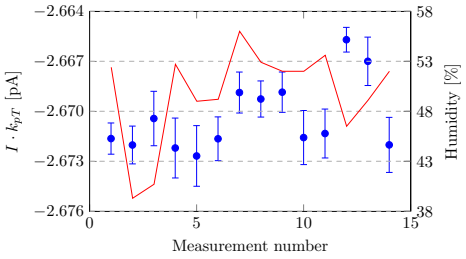

(a) Changes of the ionization current with k_{pT} correction for ^{137}Cs beam according to humidity (red line).

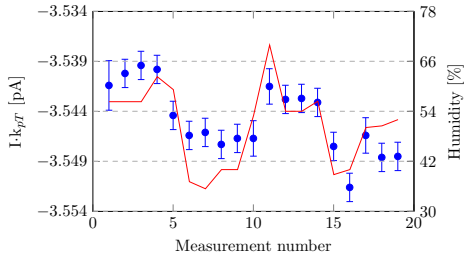

(b) Changes of the ionization current with k_{pT} correction for ^{60}Co beam according to humidity(red line).

Fig. 8. Relative humidity during mid-term stability measurements. Error bars represent expanded uncertainty with coverage factor of 2. (For interpretation of the references to colour in this figure legend, the reader is referred to the web version of this article.)

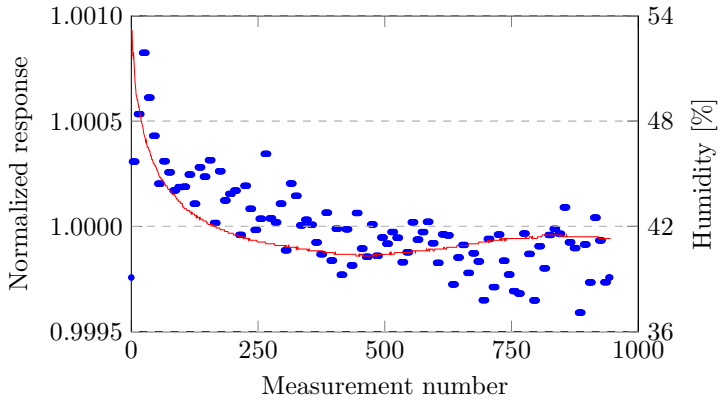

Fig. 9. Relative humidity (red line) during short-term stability measurements for ^{60}Co source. (For interpretation of the references to colour in this figure legend, the reader is referred to the web version of this article.)

For 1 m distance the attenuation corrector factor various from 0.9998 to 0.99996 for ^{137}Cs beam, and from 0.9998 to 0.9999 for ^{60}Co. Hence it can be consider as negligible, therefore $k_{att} = 1$.

4.3. Stem scatter correction

The stem effect has to be considered in order to exclude photons from an irradiated stem that reach collecting volume and influence an overall chamber response. Stem correction is introduced as the ratio of the ionization current without and with the dummy stem: $k_{stem} = I_{nostem}/I_{stem}$. The experimental setup is presented in Fig. 10. To measure I_{stem}, the dummy stem was placed on the top of the prototype chamber cap. Measurements of the ionization current without and with the stem were carried out twice. Each time the leakage current was measured and taken into account. Value of k_{stem} was quantified for both sources. Final result is a mean value of two measurements and the results for ^{137}Cs and ^{60}Co source are respectively: $k_{stem}^{Cs} = 0.9966$ and $k_{stem}^{Co} = 0.9982$, both with 0.1% uncertainty (which is an standard deviation).

4.4. Ion recombination correction

The ion collection efficiency is an issue of two separate effects: initial and volume recombination. The initial component is related to the recombination of ions from the same secondary electron path and it is independent of a dose rate. The volume recombination involves ions produced in different tracks and thought it is dose rate dependent. The mechanisms of both types of recombination is explained in chapter 12.4.4 [7]. Several methods can be use to calculate recombination factor k_{rec}. Method introduced by de Almeida and Niatel in [8] and summarized by Boutillon in [9] describes recombination correction factor as:

$$k_{rec} \approx 1 + \frac{A}{|V|} + \frac{B}{|V|^2}|I_V| \tag{9}$$

where I_V is the measured ionization current for applied voltage V, A and B are constants characterizing the ionization chamber and the beam. $A|V|^{-1}$ is an initial recombination contribution and $B|V|^{-2}$ stands for volume recombination factor. A and B can be obtained by measuring ionization current for different voltages (V and V/m) and different kerma rates. That leads to a linear relation between ratio $I_V/I_{V/m}$ and the ionization current I_V, given by:

$$\frac{I_V}{I_{V/m}} \approx 1 + (m-1)\frac{A}{|V|} + (m^2-1)\frac{B}{|V|^2}|I_V| \tag{10}$$

Knowing the slope of the line (from linear Eq. (10)) and the adequate Y-intercept value, constants A and B are possible to determine.

The current was measured at several different values of kerma rates by using thick lead plates (covered from the chamber side with 0.5 mm aluminum) to decrease radiation rate. The applied voltages were $V = 300$ V and $\frac{V}{m} = 100$ V (ergo m = 3) for both polarities.

Results for ^{137}Cs and ^{60}Co beam are presented in Fig. 11. I_V is the mean value of the ionization current for +300 V and −300 V, including leakage current and without any corrections. Values in the ratio $I_V/I_{V/m}$ are also mean values for the ionization current

Fig. 10. Experimental setup for stem effect measurements: the dummy stem (left) and the prototype chamber with dummy stem on (right).

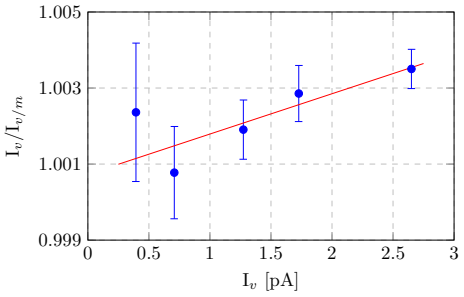

(a) Determination of recombination correction for ^{137}Cs source.

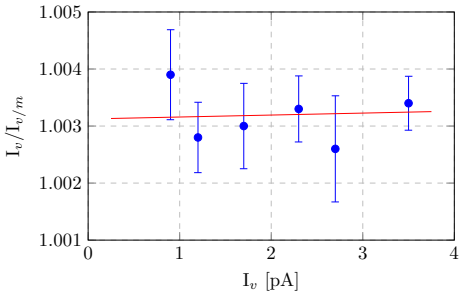

(b) Determination of recombination correction for ^{60}Co source.

Fig. 11. Linear fit to the ratio $I_V/I_{V/m}$ as a function of I_V. Error bars represent standard uncertainty.

for both polarities of 300 V and 100 V, but with pressure and temperature correction.

Results are presented in Table 3. Overall uncertainty for k_{rec} was calculated as a propagation of slope and Y-intersect uncertainty.

5. Monte Carlo simulations

5.1. Description of Monte Carlo methods

Some of the coefficients and corrections factors in the Bragg-Gray model of air kerma K are obtained by means of Monte Carlo methods. In this work the following EGSnrc codes [10–12] were used:

- CAVRZnrc for calculations of correction factors k_{wall} and k_{an} representing the graphite-wall effects on incoming radiation and axial non-uniformity of radiation, respectively.
- SPRRZnrc for stopping power ratio $\bar{s}_{c,a}$ calculation.
- the user code 'g' for evaluation of the ratio of mass energy absorption coefficients $(\bar{\mu}_{en}/\rho)^{air}_{wall}$ and the mean fraction of electron energy lost due to radiative processes while slowing in air (so called bremsstrahlung) $\bar{g}_{air}$.

Default settings for the 'Transport parameters' were used, as they fit best for the cylindrical type of chamber which was analyzed. Rogers and Kawrakow showed that the default settings of simulations generate the results of D, k_{wall}, k_{an} and $s_{c,a}$ that have the average value with reference to other results which are obtained when different parameters are changed [12]. The number of iterations was set to 10^9. Spectrum files were used for ^{60}Co and ^{137}Cs that are provided with the codes. The model of the cavity chamber that is needed in the CAVRZnrc code is presented in Fig. 12. The correction factor k_{wall} for wall effects is evaluated by the code as a combination of two factors: $k_{wall} = k^{(g)}_{att} k^{(g)}_{sc}$ where [13]:

$$k^{(g)}_{att} = \frac{D_{noatt,noscatt}}{D_{noscatt}} \tag{11}$$

is the effect of a photon attenuation in graphite and

$$k^{(g)}_{sc} = \frac{D_{noscatt}}{D_{real}} \tag{12}$$

is the effect of photon scattering in wall material. The subscripts 'noatt' and 'noscatt' means that absorbed dose to cavity gas D is calculated in the absence of attenuation and scattering of photons, respectively. The absorbed dose and k_{wall} was obtained for parallel beam ('src10') and point source ('src11') placed at a distance of

Table 3
Results obtained from linear fit for ^{137}Cs and ^{60}Co source.

	Slope	Y-intersect	Initial part	Volume part	k_{rec}	$u_{k_{rec}}$
^{137}Cs	1.06E−03	1.0007	3.65E−04	1.32E−04	1.0004	0.03%
^{60}Co	3.43E−05	1.0031	1.56E−03	4.29E−06	1.0016	0.02%

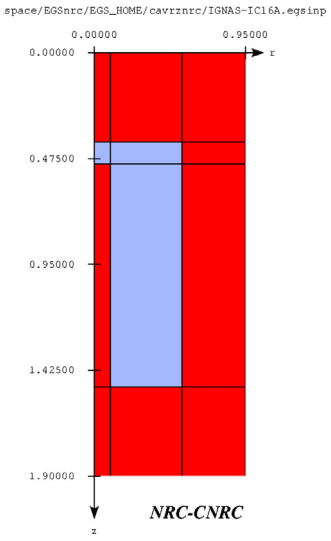

Fig. 12. Chamber model in the CAVRZnrc code.

100 cm from the center of the cavity. This allows to calculate the correction factor k_{an} which is defined as [14]:

$$k_{an} = \frac{D^{parallel}_{noatt,noscatt}}{D^{point}_{noatt,noscatt}} \tag{13}$$

but more suitable formulation of this fraction is [12]:

$$k_{an} = \frac{(D_{real}k_{wall})^{parallel}}{(D_{real}k_{wall})^{point}} \tag{14}$$

as it contains the data obtained from CAVRZnrc simulations. The product of two factors k_{an} and k_{rn} discussed earlier gives the full correction $k_{pn} = k_{an}k_{rn}$ for point-source non-uniformity. Although real sources have finite sizes and are rather of cylindrical shape, various publications show that simulating point source is sufficient [12]. The mass energy absorption coefficients $(\bar{\mu}_{en}/\rho)_i$ where $i = \{air, wall\}$ and the mean fraction of electron energy lost due to bremsstrahlung $\bar{g}_{air}$ are evaluated by the 'g' code in two separate simulations for two materials of interest. The spectral mean value is understood as energy-fluency-weighted integrated average [4]:

$$\bar{\mu}_{en}/\rho = \frac{\int \psi_E(\mu_{en}/\rho)dE}{\int \psi_E dE} \tag{15}$$

and

$$\bar{g}_{air} = \frac{\int \psi_T g_{air}(T)dT}{\int \psi_T dT} \tag{16}$$

where ψ_E is energy fluence of photons and ψ_T is energy fluence of primary electrons of initial kinetic energy T. Both $(\bar{\mu}_{en}/\rho)_i$ and $\bar{g}_{air}$ were calculated for default parameters of the 'g' user code.

In a case of the stopping-power $s_{c,a}$ simulations with SPRRZnrc code are made. It is based on the Spencer-Attix model with photon regeneration [15]:

$$\bar{s}_{c,a} = \left(\bar{S}/\rho\right)_{c,a} = \frac{\int_{\Delta}^{T_{max}} \psi_T (L(T,\Delta)/\rho)_c dT + (S_{col}(\Delta)/\rho)_c \psi_T(\Delta)\Delta}{\int_{\Delta}^{T_{max}} \psi_T (L(T,\Delta)/\rho)_{air} dT + (S_{col}(\Delta)/\rho)_{air} \psi_T(\Delta)\Delta} \tag{17}$$

where $(S_{col}(\Delta)/\rho)$ is the unrestricted mass collision stopping power $(L(T,\Delta)/\rho)$ is the restricted stopping power and Δ is the kinetic energy of electron which would have a mean chord range in air equal to $l = 4V/S$ where V is the volume and S is the surface area of the air cavity [16]. That is why most calculations for the chamber similar to these presented in the paper are done with Δ (denoted in the EGSnrc codes as 'ECUT') equal to 10 keV. It is also important to turn the photon regeneration on to eliminate the effect of photon scattering. Since the recommended value of $(W/e)_{air}$ equal to 33.97 JC^{-1} was used, it is important to choose the appropriate value of the ionization potential $I = 81$ eV and the value of graphite grain density $\rho = 2.265$ g/cm^3 (including the effect of electron screening in the material) for the $\bar{s}_{c,a}$ simulations, because there were some controversies shown that different $\bar{s}_{c,a}$ evaluation does not agree with the value of the product of the two coefficients $(W/e)_{air}s_{c,a}$ and what really matters in the model of air kerma K is the value of this product [4].

5.2. Results of the calculations

The values of correction factors k_{wall} and k_{an} for ^{60}Co and ^{137}Cs spectrum are listed in Table 4. All these values were obtained with the presence of the central electrode. If we include the influence of the electrode in the separate correction factor k_{cel} and simulate k_{wall} with whole air cavity (filling the electrode region in the CAVRZnrc code with air but keeping it as separate region), the value of the product $k_{cel}k_{wall}k_{an}$ is the same so this separation of k_{cel} is not necessary. Summary of the material constants evaluated with EGSnrc as well as with the new approach according to the new ICRU90 Report [17] are presented in Tables 5 and 6. The mean fraction

Table 5
Results obtained with the 'g' user code.

Source	$\bar{g}_{air}$	$u(\bar{g}_{air})$	$\left(\mu/\rho_{c,a}\right)$	$u\left(\mu/\rho_{c,a}\right)$
^{137}Cs	0.0014	0.02%	0.9994	0.03%
^{60}Co	0.0029	0.02%	0.9990	0.03%

Table 6
Discussion over the values of W_{air} and $s_{c,a}$.

Source	W_{air}/eV	$u(W_{air})$	$\bar{s}^{old}_{c,a}$	$u\left(\bar{s}^{old}_{c,a}\right)$	$\bar{s}^{new}_{c,a}$	$u\left(\bar{s}^{new}_{c,a}\right)$
^{137}Cs	33.97	0.15%	1.0101	0.10%	1.0023	0.08%
^{60}Co	33.97	0.15%	1.0011	0.10%	0.9928	0.08%

Table 4
Correction factors k_{wall} and k_{an}.

Source	D/Gy	$u(D)$	k_{wall}	$u(k_{wall})$	k_{an}	$u(k_{an})$
^{137}Cs src 10[a]	2.77380E−12	0.05%	1.030550	0.01%	0.99960	0.07%
^{137}Cs src 11[b]	2.77970E−12	0.05%	1.028740	0.01%		
^{60}Co src 10	4.42330E−12	0.03%	1.022890	0.01%	0.99996	0.05%
^{60}Co src 11	4.42670E−12	0.03%	1.022140	0.01%		

[a] Parallel beam incident.
[b] Point source incident.

$\bar{g}_{air}$ is needed for air only and the value obtained from the simulation agrees with that announced in previous publications [18].

Obtained results of stopping-power ratios were compared with the recommendations of the new ICRU Report. The value of $\bar{s}_{c,a}^{new}$ were recalculated by Burns [19] using his approximated empirical relations, which in case of ^{60}Co is in the following form:

$$\bar{s}_{c,a}^{new} = 1.1202 - I_c/636 \quad (18)$$

where the accepted value of the ionization potential for graphite is I_c = 81 eV. He also formulated the correction factor k_{bulk} to include different values of bulk density of graphite:

$$k_{bulk} = 1.0091 - 0.0040\rho_c \quad (19)$$

However, since the recommended value of W_{air} does not change, the minimal uncertainty for the product $s_{c,a}W_{air}$ is obtained when we do not include k_{bulk} and thus the calculation of $\bar{s}_{c,a}^{new}$ is based only on the value of crystalline density of graphite.

6. Discussion and conclusions

Table 7 summarizes the prototype chamber characteristic and correction factors obtained from measurements and results of Monte Carlo calculations for ^{137}Cs and ^{60}Co sources. Values from the table are used to calculate air kerma rate that can be compare to the present GUM primary standard (as is described in 6.1), therefore the ICRU90 Report recommendations are not included in this table.

6.1. Internal comparison to GUM standards

The prototype ionization chamber has been used to evaluate air kerma rate in ^{137}Cs and ^{60}Co source at given reference point and at a given time. Results were compared to the present GUM primary air kerma standard (cylindrical graphite-walled cavity chamber type ND1005-8303 constructed at Orszagos Mérésügyi Hivatal/MKEH in Hungary, of nominal volume of 1.013 cm^3) and summarized in Table 8. The IGNAS-IC16A#001 chamber measurements margin for present primary kerma standard is 0.11% over a standard for ^{137}Cs beam and 0.50% below the standard for ^{60}Co beam.

According to the last international comparisons [20] (with present GUM primary standard) if the potential primary standard IGNAS-IC16A#001 was compared to BIPM standard the deviation would be less then 0.25%. Particularly for ^{137}Cs beam the difference is 0.05% and for ^{60}Co beam it is −0.24%. These estimations are planned to be confirmed during next key comparisons.

6.2. Re-evaluation of the standard according to the recommendations of ICRU90 Report

According to newest ICRU90 Report [17] the corrections factors for air kerma standard have to be revised. Details were described in Section 5. Air kerma rate for the prototype chamber was calculated using modified values as summarized in Table 9. New physical constants and correction factors move IGNAS-IC16A#001 potential primary standard below present GUM standard: 0.6% for ^{137}Cs and 1.31% for ^{60}Co beam. The difference between values of revised air kerma rate $\dot{K}_{air}^{new}$ and air kerma rate calculated with old physical constants $\dot{K}_{air}$ stands at 0.71% for ^{137}Cs and 0.81% for ^{60}Co beam.

6.3. Closing remarks

In this work the new graphite-walled ionization chamber IGNAS-IC16A#001 was introduced and characterized. The proto-

Table 8
Calculated air kerma rate for the prototype chamber with comparison to GUM primary standard.

Source	$\dot{K}_{air}/(Gy/s)$	$u(\dot{K}_{air})$	$\dot{K}_{ref}/(Gy/s)$	$\dot{K}_{air}/\dot{K}_{ref}$
^{137}Cs	7.6336E−05	0.29%	7.6253E−05	1.0011
^{60}Co	1.0025E−05	0.29%	1.0075E−05	0.9950

Table 7
The prototype chamber characteristic- physical constants and correction factors with their estimated relative uncertainty for air kerma rate calculations.

	^{137}Cs source			^{60}Co source		
		Uncertainity[a]			Uncertainity[a]	
	Values	Type A	Type B	Values	Type A	Type B
Chamber parameters						
chamber volume V/cm^3	1.0191		0.15[c]	1.0191		0.15[c]
ionization current I/pA[b]	2.6704	0.08	0.02	3.5448	0.10	0.02
Physical constants						
dry air density $\rho_0/\frac{kg}{m^3}$	1.2045		0.01	1.2045		0.01
mean energy to produce an ion pair W_{air}/eV	33.9700		0.15	33.9700		0.15
mass energy absorption coefficient ratio[d] $(\bar{\mu_{en}}/\rho)_{air,c}$	0.9990		0.05	0.9985		0.05
stopping power $\bar{s}_{c,a}$	1.0101		0.10	1.0011		0.10
bremsstrahlung loss[d] $\bar{g}_{air}$	0.0012		0.02	0.0032		0.02
Measured correction factors						
humidity k_h	0.9970		0.03	0.9970		0.03
recombination losses k_{rec}	1.0004		0.03[c]	1.0016		0.02[c]
stem scattering k_{stem}	0.9966	0.11		0.9982	0.10	
Calculated correction factors						
wall attenuation and scattering k_{wall}	1.0287		0.01	1.0221		0.01
axial non-uniformity k_{an}	0.9996		0.07	1.0000		0.05
radial non-uniformity k_{rn}	1.0002		0.02	1.0002		0.02
Relative standard uncertainty						
quadratic summation		0.13	0.21		0.14	0.20
combined uncertainty			**0.29**			**0.29**

[a] Relative non-expanded uncertainty in percentage.
[b] The ionization current with applied correction for pressure and temperature $k_{p,T}$.
[c] Combined uncertainty.
[d] Values according to GUM primary standard [20].

Table 9
The new values for air kerma rate calculations according to ICRU90 Report and calculations from Table 5.

	^{137}Cs source			^{60}Co source		
		Uncertainity[a]			Uncertainity[a]	
	Values	Type A	Type B	Values	Type A	Type B
W_{air}/eV	33.97		0.35	33.97		0.35
$(\bar{\mu_{en}}/\rho)_{air,c}$	0.9994		0.03	0.9990		0.03
$\bar{s}_{c,a}$	1.0023		0.08	0.9928		0.08
$\bar{g}_{air}$	0.0014		0.02	0.0029		0.02
	Revised air kerma rate calculations					
$\dot{K}_{air}^{new}/(Gy/s)$	7.5792E−05			9.9435E−05		
$u\left(\dot{K}_{air}^{new}\right)$	0.42%			0.42%		
$\dot{K}_{ref}/(Gy/s)$	7.6253E−05			1.0075E−05		
$\dot{K}_{air}^{new}/\dot{K}_{ref}$	0.9940			0.9869		

[a] Relative non-expanded uncertainty in percentage.

type chamber was tested during various measurements and its reliability as an air kerma standard for ^{137}Cs and ^{60}Co gamma sources was proved. All measured and discussed correction factors implicate good quality of the chamber. The air kerma rate obtained with IGNAS-IC16A#001 chamber is in a satisfactory consistency with the present GUM kerma standard and should give a high compliance with international standards. Therefore the prototype chamber described and characterized in this paper is a highly recommended as a new GUM air-kerma primary standard.

Acknowledgments

The authors acknowledge R. Andrzejczak for multi-tooling, machining and other helpful inevitable works on building and developing standards in our laboratory.

Development of the prototype chamber was supported by knowledge and experience from the EMPIR Project 14RPT04 ABSORB.

References

[1] F. Delaunay, M. Donois, J. Gouriou, E. Leroy, A. Ostrowsky, New LNHB primary standard for 60 Co air kerma, Metrologia 47 (6) (2010) 652.
[2] M.-M. Bé, et al., Table of Radionuclides, Vol. 8 of Monographie BIPM-5, Bureau International des Poids et Mesures, Sévres, 2016.
[3] P. Andreo, D.T. Burns, K. Hohlfeld, M.S. Huq, T. Kanai, F. Laitano, V.G. Smyth, S. Vynckier, Absorbed Dose Determination in External Beam Radiotherapy, Technical Reports Series 398, International Atomic Energy Agency, Vienna, 2001.
[4] L. Büermann, D.T. Burns, Air-kerma cavity standards, Metrologia 46 (2) (2009) S24, URLhttp://stacks.iop.org/0026-1394/46/i=2/a=S03.
[5] S.M. Seltzer, P.M. Bergstrom Jr., Changes in the U.S. primary standards for the air kerma from gamma-ray beams, J. Res. Natl. Inst. Stand. Technol. 108 (5) (2003) S359.
[6] M.R. Mc Ewen, J. Taank, Examining the influence of humidity on reference ionization chamber performance, Med. Phys. 44 (2) (2017) 694–702.
[7] P. Andreo, D.T. Burns, A.E. Nahum, J. Seuntjens, F.H. Attix, Fundamentals of Ionizing Radiation Dosimetry, Wiley, 2017, URLhttps://books.google.pl/books?id=tKfDoQEACAAJ.
[8] C.E. de Almeida, M.T. Niatel, Comparison between IRD and BIPM exposure and air kerma standards for cobalt gamma rays, Rapport BIPM 1986/12, Bureau International des Poids et Mesures, Sévres, 1986.
[9] M. Boutillon, Volume recombination parameter in ionization chambers, Phys. Med. Biol. 43 (8) (1998) 2061, URLhttp://stacks.iop.org/0031-9155/43/i=8/a=005.
[10] I. Kawrakow, D.W.O. Rogers, The EGSnrc code system: Monte Carlo simulation of electron and photon transport, Technical Report PIRS-701, National Research Council of Canada, Ottawa, 2000.
[11] D.W.O. Rogers, I. Kawrakow, J.P. Seuntjens, B.R.B. Walters, The possibility of a universal social welfare function, Technical Report PIRS-702, National Research Council of Canada, Ottawa, 2000.
[12] D.W.O. Rogers, I. Kawrakow, Monte Carlo calculated correction factors for primary standards of air kerma, Med. Phys. 30 (4) (2003) 521–532, URLhttps://aapm.onlinelibrary.wiley.com/doi/abs/10.1118/1.1563663.
[13] A.F. Bielajew, Ionisation cavity theory: a formal derivation of perturbation factors for thick-walled ion chambers in photon beams, Phys. Med. Biol. 31 (2) (1986) 161, URLhttp://stacks.iop.org/0031-9155/31/i=2/a=005.
[14] A.F. Bielajew, An analytic theory of the point-source nonuniformity correction factor for thick-walled ionisation chambers in photon beams, Phys. Med. Biol. 35 (4) (1990) 517, URLhttp://stacks.iop.org/0031-9155/35/i=4/a=004.
[15] A.E. Nahum, Water air stopping-power ratios for megavoltage photon and electron beams, Phys. Med. Biol. 23 (1) (1978) 24.
[16] F.H. Attix, Introduction to Radiological Physics and Radiation Dosimetry, Wiley, New York, 1986.
[17] ICRU, ICRU Report 90: Key Data For Ionizing-Radiation Dosimetry: Measurement Standards And Applications, Vol. 14 of Journal of the ICRU, Oxford University Press, Oxford, 2014.
[18] D.T. Burns, A new approach to the determination of air kerma using primary-standard cavity ionization chambers, Phys. Med. Biol. 51 (4) (2006) 929, URLhttp://stacks.iop.org/0031-9155/51/i=4/a=012.
[19] D. Burns, C. Kessler, Re-evaluation of the BIPM international dosimetry standards on adoption of the recommendations of ICRU Report 90, Metrologia 55 (4) (2018) R21, URLhttp://stacks.iop.org/0026-1394/55/i=4/a=R21.
[20] P.J. Allisy-Roberts, C. Kessler, D.T. Burns, M. Derlaciński, J. Kokociński, Comparisons of the standards for air kerma of the GUM and the BIPM for 60 Co and 137 Cs gamma radiation, Metrologia 48 (1A) (2011) 06015, URLhttp://stacks.iop.org/0026-1394/48/i=1A/a=06015.